Comparison of the Ca + HF(DF) and Sr + HF(DF) reaction dynamics

Rong Zhang, David J. Rakestraw,[a] Kenneth G. McKendrick,[b] and Richard N. Zare
Department of Chemistry, Stanford University, Stanford, California 94305-5080

(Received 19 July 1988; accepted 2 August 1988)

A comparative study of the reaction family, Ca and Sr with rovibrationally selected HF or DF, has been carried out under single-collision conditions. A thermal beam of the alkaline earth atoms, Ca or Sr, is fired into a low-pressure gas of HF or DF in which the reagent molecules have been prepared in a selected vibration–rotation state by the use of a tunable infrared light source (optical parametric oscillator). The resulting alkaline earth monofluoride reaction products, CaF or SrF, are detected in a quantum-state-specific manner with a tunable visible light source (dye laser) using laser induced fluorescence. The HF molecule is aligned with its rotational angular momentum pointing preferentially either along or perpendicular to the metal atom beam. For both Ca + HF($v = 1$) and Sr + HF($v = 1$) the cross section and the product state distribution are found to be independent of the approach geometry, which is consistent with reaction through a bent transition state. The state-to-state reaction dynamics for Ca + HF(DF) and Sr + HF(DF) show marked differences. The Ca + HF(DF) → CaF + H(D) reaction has attributes of a statistical internal energy distribution, whereas Sr + HF(DF) → SrF + H(D) shows some deviation from this behavior. The findings for Ca + HF(DF) are consistent with a model in which the Ca atom inserts into the HF bond to form a long-lived H–Ca–F intermediate; the findings for Sr + HF(DF) are interpreted as competition between direct reaction and reaction which samples the deep H–Sr–F potential well.

I. INTRODUCTION

Over the past 15 years, laser induced fluorescence (LIF) has made possible the detailed study of the reactions of alkaline earth metal atoms M with hydrogen fluoride molecules HF

$$M + HF \rightarrow MF + H. \quad (1)$$

Specific reactions investigated under single-collision conditions include the exoergic reaction Ba + HF,[1–5] and the increasingly endoergic reactions Sr + HF[6–10] and Ca + HF.[6,11] The latter two reactions require either vibrational excitation of the HF reagent or hyperthermal translational energy of the collision partners for the reactions to proceed.

The dynamics of this reaction family are quite interesting. Because of the mass combination, heavy + heavy–light to form heavy–heavy + light, orbital angular momentum of the collision is expected to be channeled almost exclusively into rotational angular momentum of the diatomic product.[12] For the Ba + HF reaction, both the effects of reagent translational energy and internal vibrational energy [HF($v = 1$) and ($v = 2$)] have been studied.[2–5] Gupta, Perry, and Zare[3] have found that this system has a small threshold energy (~ 1 kcal/mol). The peak of the BaF vibrational distribution is at $v = 1$ for the thermal beam–gas reaction. As the collision energy is increased, the total cross section for this reaction rises and then falls. At the same time, the peak of the vibrational distribution moves to higher vibrational levels (an inverted vibrational distribution) and then returns to $v = 0$. This inverted vibrational distribution is considered to be evidence for a "direct reaction." Torres-Filho and Pruett[5] have found that the product distribution is essentially the same whether reagent vibration or reagent translation is utilized. This is one characteristic of what is regarded as statistical behavior. Thus, in terms of direct reaction vs reaction via a complex, it is not clear how to classify the Ba + HF system.

In contrast, previous investigations showed that the behavior of the Ca + HF reaction system is clearly statistical in terms of partitioning of energy among the product states, independent of the form of the reagent energy. The effect of reagent rotation on the product vibrational state distribution has been reported for Ca + HF($v = 1, J = 0$–7) by Altkorn *et al.*[11] They found that the CaF internal state distribution can be modeled by an "unbiased" prior distribution in which the excess energy of reaction is disposed statistically into all possible modes. This conclusion holds over a large range of reagent internal energies. In that study, the maximum rotational energy introduced is comparable to the average energy available to the HF($v = 1$) rotationless reagents. Recently, a first principles investigation of this reaction was carried out by Jaffe *et al.*[13] This study shows that a deep H–Ca–F potential energy well dominates the collision dynamics of Ca + HF. For example, at a relative initial kinetic energy of 5 kcal/mol, more than 98% of the trajectories sample this well. Thus, the Ca + HF reaction constitutes a prototype of a neutral three-atom chemical insertion reaction which proceeds through a long-lived complex. Although individual trajectories appear to be non-RRKM in the classical sense of fully exploring phase space, the averaging over initial conditions gives a product distribution that is close to statistical.

An obvious question is whether the Sr + HF reaction dynamics is better described as statistical (like Ca + HF) or

[a] Present address: Sandia National Laboratory, Division 8362, P.O. Box 969, Livermore, California 94551-0969.
[b] Present address: Department of Chemistry, University of Edinburgh, West Mains Road, Edinburgh EH9 3JJ, United Kingdom.

direct (like some aspects of Ba + HF). The comparison of reagent translation with reagent vibration has been studied by Gupta, Perry, and Zare[9] for the Sr + HF system. The cross section of the Sr + HF ($v = 1$) reaction is found to be about 1–10 times greater than that of the Sr + HF ($v = 0$) reaction when the same total energy is supplied as reagent translation. By analogy with the studies of Polanyi *et al.*,[14] in which it was inferred that vibration may be two to three orders of magnitude more effective than translation in promoting a number of substantially endothermic reactions, Gupta *et al.* suggested that reagent vibration was less effective than what would be expected in a direct reaction of Sr with HF. They also found that the product state distribution seemed to be in agreement with phase space theory, i.e., it was statistical. The effects of reagent rotation were studied by Man and Estler,[10] who investigated Sr + HF($v = 1, J$) over the limited range $J = 1$–3. They observed that the SrF vibrational state distributions could also be interpreted as agreeing with the predictions of phase space theory. Gupta *et al.*[9] suggested that this reaction proceeds by "snarled" trajectories causing some observables to be statistical, but a more complete description was lacking.

We report here a comparative investigation of the role of reagent rotation and vibration on the product internal state distributions for the reactions Ca + HF($v = 1, J = 0$–7), Ca + DF($v = 1, J = 0$–$9; v = 2, J = 1$–5), Sr + HF($v = 1, J = 0$–7), and Sr + DF($v = 1, J = 0$–$9; v = 2, J = 1$–5). The reactions Ca + HF ($v = 1$, $J = 0$–7) were studied previously in this laboratory several years ago.[11] We have repeated this study and the results are similar to those of Altkorn *et al.*[11] In the present and previous studies, reagent vibrational and rotational states are selected by excitation via the tunable infrared output from an optical parametric oscillator. The CaF and SrF products are detected by laser-induced fluorescence (LIF).

We find dramatic differences between the reaction dynamics of Ca and Sr. Whereas Ca + HF(DF) behaves statistically, Sr + HF(DF) shows clear departures from such a description. A sensitive test is to compare the product state distribution for reaction with HF($v = 1, J = 7$) and DF($v = 2, J = 1$) because these two reagents have almost the same total internal energy. We find that Sr + HF($v = 1, J = 7$) differs from Sr + DF($v = 2, J = 1$), whereas the analogous Ca reactions give essentially the same product state distribution. We offer an interpretation for this behavior in which the reaction of a strontium atom with a hydrogen fluoride molecule involves the competition between a direct abstraction reaction and an insertion reaction which proceeds through a complex.

II. EXPERIMENTAL PROCEDURE AND DATA ANALYSIS

A. Pump–probe configuration

Figure 1 shows a schematic diagram of the apparatus. We use a counterpropagating "pump–probe" geometry in which a tunable IR laser pumps HF/DF reagents and a tunable dye laser probes alkaline earth monofluoride products. The beam–gas reactor consists of an oven chamber and a scattering chamber which are separated from each other by an aluminum wall having a 0.3×2.5 cm rectangular slit. This slit, located 6 cm from the oven orifice and 2.5 cm from the scattering center, provides final collimation of the metal atom beam. Each chamber is individually evacuated by a 6 in. oil diffusion pump. The background pressure with the oven on is about 1×10^{-5} Torr for the oven chamber and 2×10^{-6} Torr for the scattering chamber, as measured by an

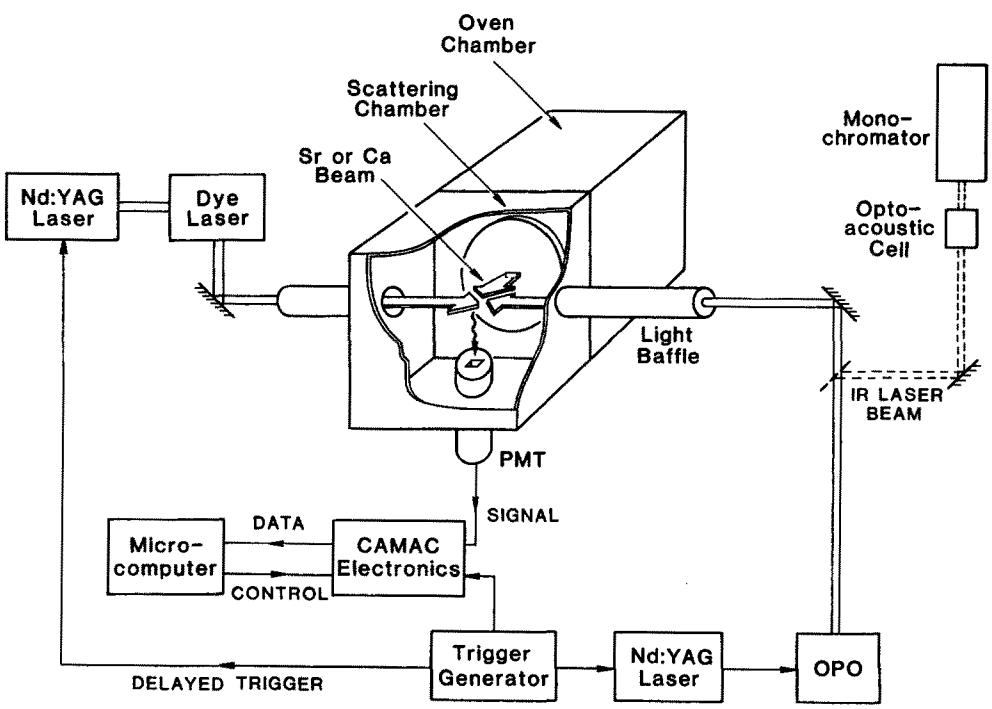

FIG. 1. Schematic diagram for pump–probe experimental arrangement.

uncalibrated ionization gauge (Granville–Phillips, model 274002). An atomic beam of the alkaline earth metals (Alfa, purity >99% both for Ca and Sr) effuses from a stainless steel crucible having an elliptical orifice of 1.0×2.5 mm. This oven is heated to about 1040 K for Sr and 1080 K for Ca which results in a vapor pressure inside the oven of around 1 Torr. The temperatures are measured by a tungsten–rhenium thermocouple and are held constant to within ± 5 K during each run.

The HF or DF gas is introduced directly into the scattering chamber through a stainless steel needle valve from a lecture bottle (Matheson, >99% stated purity). The pressure in the scattering chamber is maintained at 0.2–0.4 mTorr. Before the gas is admitted to the chamber, the bottle is placed into a liquid nitrogen trap in order to freeze the HF/DF gas, thus allowing volatile impurities to be pumped out. During the experiments the gas reservoir is maintained at 273 K using an ice-water bath to ensure a stable backing pressure.

The infrared pump beam is produced by an optical parametric oscillator (OPO) and brought to a loose focus at the scattering center (spot size ~3 mm) with a 2 m focal length gold coated mirror. The OPO consists of an angle-tuned $LiNbO_3$ crystal pumped in the far field by a Nd:YAG laser (Quanta-Ray DCR-1) which has a 15 ns pulse width. The OPO is tunable over the range of 1.4–4.2 μm with ~5–10 mJ/pulse of energy and a bandwidth of 0.1–0.2 cm^{-1} when operating with an intracavity etalon. Because HF or DF fundamental transitions have large absorption cross sections (approximately 10^{-15} cm^2),[15] they are easily saturated. Therefore, when HF($v=1$) or DF($v=1$) is prepared, the brightness of the IR radiation from the OPO is decreased by removing the intracavity etalon. The resulting OPO bandwidth becomes ~1.0 cm^{-1}. A crude check revealed that under these conditions the reaction product yield was linear with the OPO power output. A monochromator (3/4 meter length with a 600 groove/mm grating; SPEX, model 2569) is used to coarse tune the OPO output to the desired wavelength. An optoacoustic cell (fitted with a transducer, PCB Piezotronics Inc., New York, model GK106B50, together with model 480D06 preamplifier) is then used to fine tune the OPO wavelength to coincide with individual HF or DF absorption lines. We also use the optoacoustic cell to determine the relative number of HF molecules prepared in a specific internal state. This information is used in measuring how the relative reaction cross section changes with reagent rotation. Excitation of HF($v=1, J$) and DF ($v=1,2; J$) is accomplished via the stronger R-branch lines except for $J=0$ in which case the $P(1)$ line is used.

Laser-induced fluorescence is excited via the MF $A\,^2\Pi$–$X\,^2\Sigma^+$ band system by tunable visible (probe) radiation in the 600–610 nm region for CaF and in the 640–660 nm region for SrF. This radiation is produced by a Nd:YAG laser (Quanta-Ray DCR-2A) pumped dye laser (Quantel TDL-50) with a spectral bandwidth of ~0.1 cm^{-1}. Since there is some CaF or SrF background arising from heterogeneous reactions inside the oven, the pump laser is operated at a pulse repetition rate of 10 Hz and the probe laser is operated at 20 Hz to allow background subtraction. The probe beam spot size (5–6 mm) is chosen to be sufficiently greater than that of the pump beam so that all species produced are detected when account is taken of the short time delay between the pump and probe laser pulses. This delay time is chosen to be about 6–8 μs. This allows the metal atoms to have sufficient time to react with excited HF/DF molecules but insufficient time for collisional relaxation of the reaction products to occur to any appreciable extent. In order to reduce the effects of radiative saturation in the CaF and SrF A–X transitions, the probe pulse energies are attenuated to as low as 1–3 μJ/pulse (measured by a Molectron J3-05 power meter) through a combination of a partial back reflection from a glass window and Glan–Taylor prisms. The latter allow variable attenuation while maintaining a fixed polarization. The laser beams propagate through internally baffled entrance and exit arms (0.4 m long). All internal surfaces were coated with a matt black paint (Zuel Corporation, St. Paul, MN) which greatly reduced the level of scattered laser light.

Fluorescence is detected perpendicular to the common propagation direction of the laser beams and the direction of the metal beam. The fluorescence is collected by a lens system ($f=5$ cm) and imaged onto the photocathode of a photomultiplier tube (RCA model 7265, 2 in. diameter, S20 photocathode). Signals are captured during a time gate of 50 ns, corresponding to approximately twice the radiative lifetime of the CaF or SrF A state.[16] The opening of the gate coincides with the start of the probe laser pulse. The data are digitized (LeCroy 2249SG ADC, CAMAC modular data bus) and passed to a microcomputer (IBM PC-XT) for storage and analysis.

B. Measurement of reagent alignment effect

By selecting the direction of the linear polarization of the OPO output, it is possible to prepare the HF reagent with its plane of rotation preferentially lying either parallel or perpendicular to the direction of the metal atom beam.[17] The relative reaction cross section and the product state distribution have been measured for these two different approach geometries. Care is taken not to saturate the HF transition, since saturation reduces the alignment. The linear polarization of the laser beam is ensured by a Glan–Taylor prism before the OPO beam enters the chamber through a CaF_2 window. The rotation of the polarization plane can be achieved simply by a half-wave plate which is mounted between the prism and the entrance window on the baffle arm.

C. Reaction energetics

The average total energy available to the products can be estimated from the following relation:

$$\langle E_{\rm tot}\rangle = E_{\rm int} - \Delta H^\circ_0 + \langle E_{\rm coll}\rangle, \qquad (2)$$

where $E_{\rm int}$ is the internal energy of reactant HF or DF referred to HF($v=0, J=0$) or DF($v=0, J=0$), ΔH°_0 is the reaction exoergicity, and $\langle E_{\rm coll}\rangle$ is the average collision energy of the reactants. Table I lists the values of the reaction exoergicities for the Ca + HF(DF) and Sr + HF(DF) reactions. Figures 2 and 3 show the relative energies of reagent and product states for the Ca + HF(DF) and Sr + HF(DF) reaction systems, respectively. The ground states of HF and DF are separated by 1.6 kcal/mol (560

TABLE I. Reaction energetics (kcal/mol).

	Ca + HF ($v=1, J=0$)	Ca + DF ($v=2, J=0$)	Sr + HF ($v=1, J=0$)	Sr + DF ($v=2, J=0$)
ΔH°_0	8.0 ± 2.0	9.6 ± 2.0	6.4 ± 1.6	8.0 ± 1.6
$\langle E_{\rm coll} \rangle$	2.6	2.7	2.0	2.1
$E_{\rm int}$	11.3	16.5	11.3	16.5
$\langle E_{\rm tot} \rangle$	5.9	9.6	6.9	10.6

cm^{-1}) because of the difference between zero point energies.

In the present beam–gas experiment the spread in collision energy is quite broad. Under our experiment conditions, the HF/DF gases follow room temperature Maxwellian velocity distributions, and the Ca or Sr effusive beam velocity flux distribution $F(v)$ can be expressed by[18]

$$F(v) \propto v^3 \exp(-mv^2/2kT), \quad (3)$$

where v denotes the speed, m the mass of the Ca or Sr atom, and T is the oven temperature. A Monte Carlo method[19] is used to calculate the relative collision velocity distribution. The results for the average collisional energy $\langle E_{\rm coll} \rangle$ are listed in Table I along with the corresponding values of $\langle E_{\rm tot} \rangle$.

From Figs. 2 and 3, as well as Table I, it is clear that all reactions involving vibrationally unexcited HF or DF are endoergic, while reactions with HF excited to the $v=1$ vibrational level and DF excited to the $v=2$ vibrational level are exoergic. Because of the uncertainty in the reaction exoergicity, reactions with DF($v=1$) may be slightly endoergic or exoergic depending on which rotational level of DF($v=1$) is prepared.

D. Determination of relative population distributions

MF product populations are deduced from LIF excitation spectra using the MF $A\,^2\Pi$–$X\,^2\Sigma^+$ band system. The MF A and X state potentials have almost the same shape and are displaced nearly vertically from one another. Consequently, the $\Delta v = 0$ progression has almost all the intensity (Franck–Condon factors are near unity) and the rotational band structure is highly congested. With our laser linewidth we are unable to resolve individual rotational lines in most cases. To make quantitative estimates of the product internal state distribution, a computer program is used to simulate the observed MF A–X excitation spectra.

The program, based on previous work in this laboratory,[20] calculates line positions for the six branches of each vibronic band using the spectroscopic constants[21–25,28–33] given in Table II in conjunction with standard spectroscopic formulas.[26] The rotational distribution for each vibrational level of the nascent product is assumed to have the form of a linear surprisal[3,27]:

$$P(v,J) = N_v P^0(v,J) \exp[-f_r \theta_r(v)/(1-f_v)], \quad (4)$$

where N_v is the vibrational weighting factor ($N_v = 1$ for a completely statistical distribution), $P^0(v,J)$ is the "prior" vibration–rotation population distribution, f_v and f_r are fractional vibrational and rotational energies, and $\theta_r(v)$ is an adjustable parameter. The form of the prior distribution is assumed to be[27]

$$P^0(v,J) = (2J+1)[\langle E_{\rm tot}(J'')\rangle (1-f_v-f_r)]^{1/2} \quad (5)$$

which reflects the rotational and translational degeneracies when a given (v,J) level is populated. Here $\langle E_{\rm tot}(J'')\rangle$ denotes the total average energy available to the reaction

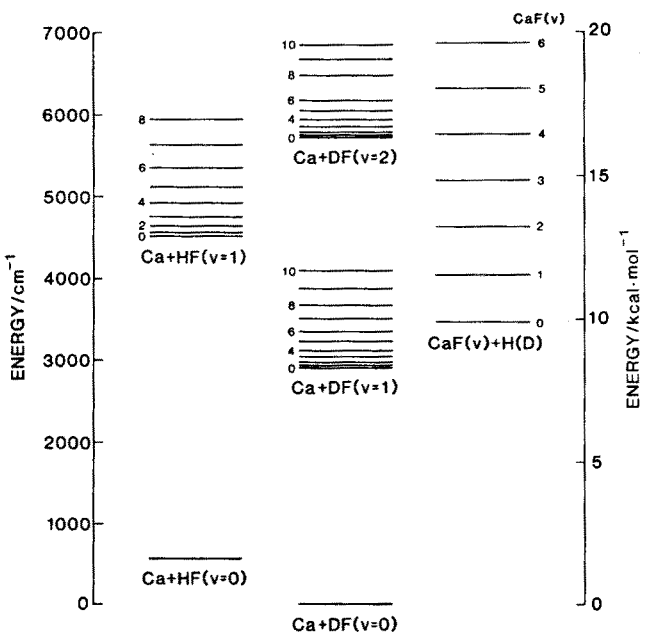

FIG. 2. Energetics for the Ca + HF(DF) reaction system. The zero reference energy is measured in the kcal/mol and in the cm^{-1} scale with respect to the DF lowest internal state. The HF(DF) levels are labeled by the rotational quantum number J.

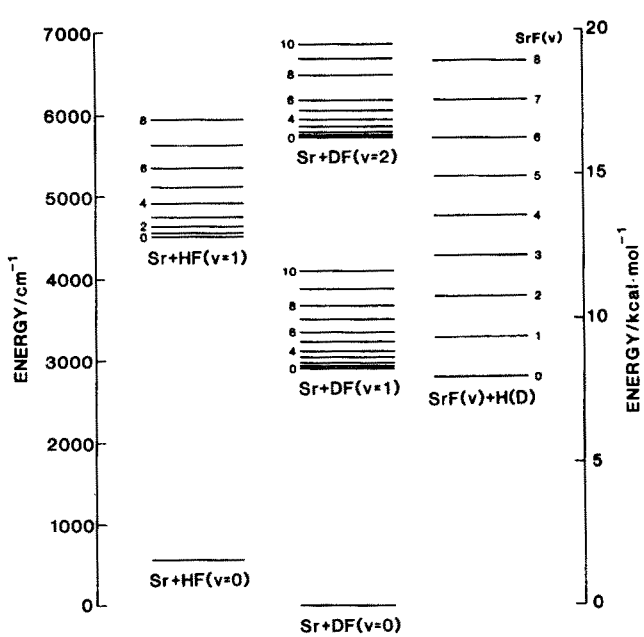

FIG. 3. Energetics for the Sr + HF(DF) reaction system. The zero reference energy is measured in the kcal/mol and in the cm^{-1} scale with respect to the DF lowest internal state. The HF(DF) levels are labeled by the rotational quantum number J.

TABLE II. CaF and SrF X and A state molecular constants (cm^{-1}).

	CaF	Ref.	SrF	Ref.
		$X\,^2\Sigma^+$ state		
ω_e	587.4	21	502.4	28
$\omega_e x_e$	2.84	21	2.27	28
B_e	0.343 704	21	0.250 53	29
α_e	0.002 436	21	0.001 546	29
D_e	4.44×10^{-7}	20	2.5×10^{-7}	28
γ_e	0.001 3	21	0.002 5	29
		$A\,^2\Pi$ state		
T_e	16 526.8	21	15 233.5[a]	27
A	71.5	21	264.3	30
ω_e	593.4	21	510.3[a]	27
$\omega_e x_e$	3.11	21	2.35[a]	27
B_e	0.348 744	21	0.253 44	30
α_e	0.002 529	21	0.001 56	30
D_e	4.55×10^{-7}	20	2.2×10^{-7}	30
p	−0.043 8	20	−0.133	30

[a] Partially adjusted to fit the spectrum from the oven reaction.

products when HF($v''=1$) or DF($v''=1,2$) is prepared in the rotational level J''. We find that the fit is improved by fixing $\langle E_{\rm tot}(J'')\rangle$ for each reaction to a value close to that expected from Table I but within the interval defined by the relatively large uncertainty in ΔH_0° (see Table IV). The

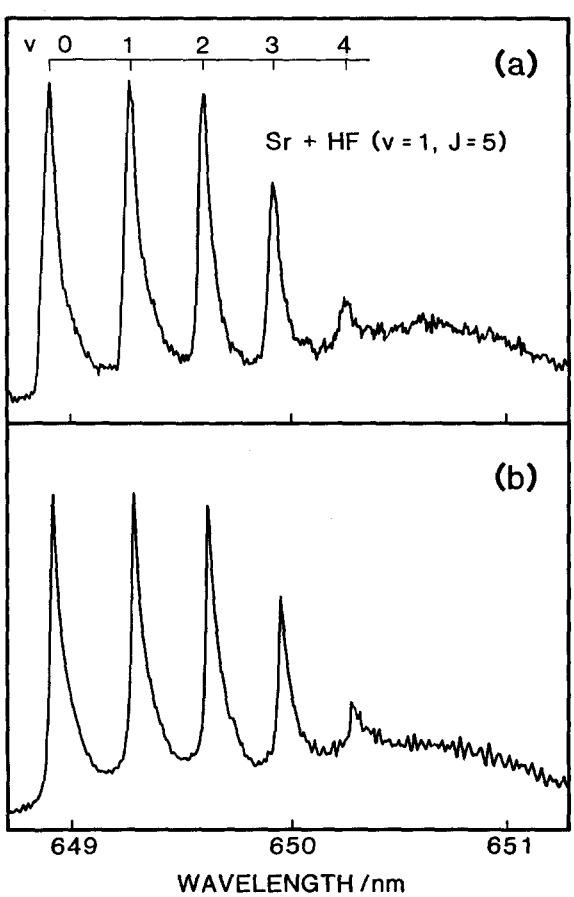

FIG. 4. LIF spectrum of the SrF $X\,^2\Sigma^+$–$A\,^2\Pi_{3/2}$ transition for the Sr + HF($v=1, J=5$) reaction: (a) experiment; and (b) simulation.

$\langle E_{\rm tot}(J'')\rangle$ is initially varied for only one value of J and all other $\langle E_{\rm tot}(J'')\rangle$ are scaled as the HF rotational energy, i.e.,

$$\langle E_{\rm tot}(J_1'')\rangle - \langle E_{\rm tot}(J_2'')\rangle = F(J_1'') - F(J_2''), \quad (6)$$

where J_1'' and J_2'' are arbitrary rotational quantum numbers for HF and F(J_i'') is the corresponding rotational term value. This quantity is then adjusted to achieve the best global fit for all values of the HF rotational quantum number.

The program convolutes each line with the laser bandwidth. To produce a simulated spectrum, the contribution of a line to the signal at a frequency is determined by the population in the (v, J) level, the Franck–Condon factor,[34] and the rotational line strength.[35] Because the laser intensity is constant over the range of the spectrum, no correction is made for its variation with wavelength. In order to take into account the experimentally unavoidable effects of saturation in the MF A–X transitions, we use a Lorentzian profile instead of a Gaussian one to describe the line shape (see the Appendix).

The simulated spectra for CaF and SrF products are derived using Eq. (4). The vibrational weights N_v and the rotational parameters $\theta_r(v)$ are iteratively adjusted, typically five to ten times, to achieve a best fit to the observed spectrum. For CaF (vide infra), the spectra are fit with $N_v=1$ and $\theta_r(v)=0$ for all v, whereas for SrF it is necessary to make full use of Eq. (4). In order to make our estimations more accurate, it is advantageous to use both the $A\,^2\Pi_{1/2}$–$X\,^2\Sigma^+$ and $A\,^2\Pi_{3/2}$–$X\,^2\Sigma^+$ subbands because the bandheads form at different rotational quantum numbers in these two subbands. Therefore, simulation of both subbands is a quite sensitive way to fix the adjustable parameters. Figure 4 gives an example of the fit obtained for the reaction Sr + HF($v=1, J=5$), which is typical of the level of agreement between simulation and observed spectra.

III. RESULTS

A. Product state distribution for Ca+HF(v=1, J=7)/DF(v=2, J=1) and Sr+HF(v=1, J=7)/DF(v=2, J=1)

The reactions of Ca with HF($v=1, J=0$–7) have been studied previously in this laboratory.[11] Following recent improvements in the experimental apparatus, we have repeated this study. We have also extended the study of this reaction system to include Ca + DF($v=2, J$). In particular, we examine the reaction of Ca + DF($v=2, J=1$) because this reaction is nearly isoenergetic with Ca + HF($v=1, J=7$) [the total energy available for Ca + DF($v=2, J=1$) is only 0.40 kcal/mol (140 cm^{-1}) greater than for Ca + HF($v=1, J=7$)]. The internal energy of the DF($v=2, J=1$) reagent consists of 16.5 kcal/mol vibrational energy and 0.06 kcal/mol rotational energy. The internal energy of the HF($v=1, J=7$) reagent consists of 11.3 kcal/mol vibrational energy and 3.2 kcal/mol rotational energy. Thus, the Ca + DF($v=2, J=1$) reaction has almost exclusively its internal energy in the form of vibrational energy, whereas the Ca + HF($v=1, J=7$) reaction has a significant fraction of its internal energy in the form of rotational energy.

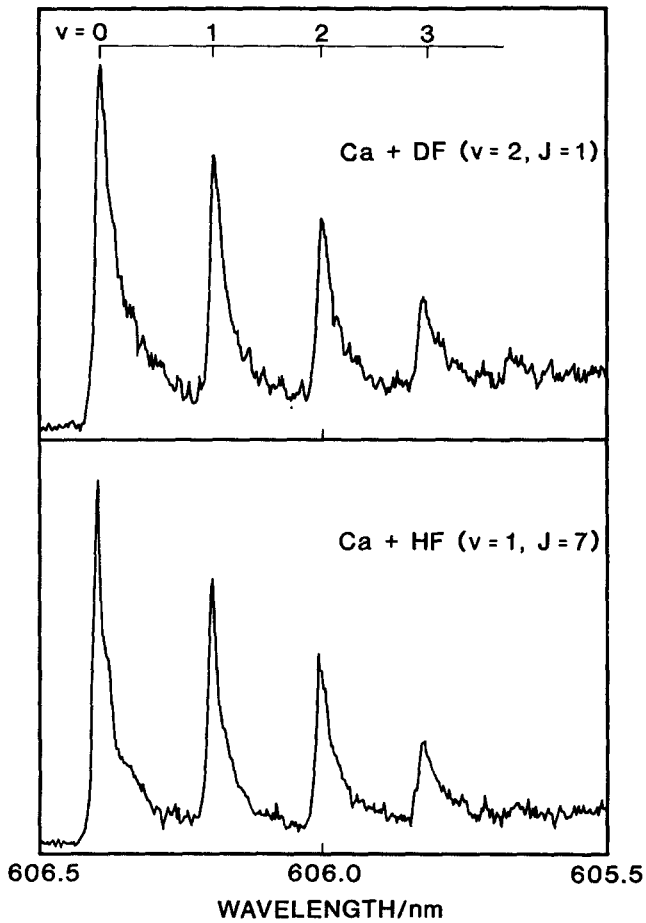

FIG. 5. LIF spectrum of the CaF $X\,^2\Sigma^+$–$A\,^2\Pi_{3/2}$ transition for the reaction: (a) Ca + DF($v = 2, J = 1$); and (b) Ca + HF($v = 1, J = 7$).

Figure 5 shows the LIF excitation spectra of CaF produced in the reactions of Ca + DF($v = 2, J = 1$) and Ca + HF($v = 1, J = 7$). It is apparent that the product state distributions are almost indistinguishable. The vibrational state distributions of the CaF products derived from these spectra are listed in Table III. The data in Table III are obtained with the prior distribution $P^0(v, J)$ shown in Eq. (5) with an angular momentum cutoff at $J = 75$. We find that the introduction of a cutoff improves the agreement between simulation and experiment. Aside from the angular momentum cutoff, this simulation corresponds to populating all energetically accessible levels in an egalitarian manner,[30] i.e., in a "statistical" distribution. As would be expected, the $P(v, J)$ decline monotonically with v, and the $\langle E_v \rangle$ (average vibrational energy in the product CaF) approximates the value calculated from the "rigid rotor harmonic oscillator" prior distribution.[36] Table III also includes the results for the Ca + HF($v = 1, J = 0$–6) and Ca + DF($v = 2, J = 3,5$) reactions which also show statistical behavior. Thus, the present study agrees with the previous study of Ca + HF($v = 1$) by Altkorn *et al.*[11]

An identical experiment has been performed with strontium. Figure 6 shows the LIF spectra from Sr + HF($v = 1, J = 7$) and Sr + DF($v = 2, J = 1$). Obviously, there is a pronounced difference. The SrF vibrational state distributions derived from these spectra are listed in Table IV. The product vibrational state distributions for the Sr + DF($v = 2, J = 1$–5) all resemble a statistical prior distribution. However, a best fit is obtained for a linear surprisal with a slope λ of 0.5 rather than zero. Similar to Ca + HF/DF, the product vibrational state distribution also decreases monotonically with the increasing product vibrational quantum number. On the other hand, the product vibrational state distribution for the Sr + HF($v = 1, J = 7$) system cannot be fit by a prior distribution or a linear surprisal. To fit the spectrum, a set of weighting factors N_v and a set of theta parameters $\theta_r(v)$ are chosen [see Eq. (4)]. The result from this best fit reveals that the vibrational state distribution for Sr + HF($v = 1, J = 7$) differs from Sr + DF($v = 2, J = 1$) in that the relative population declines less rapidly with the product vibrational quantum number.

TABLE III. Relative vibration state population of the CaF product P_v with the average total available energy $\langle E_{\rm tot}(J) \rangle$ and its energy partitioning from the Ca + HF($v = 1, J$) and Ca + DF($v = 2, J$) reactions.

	P_v									
J	$v=0$	$v=1$	$v=2$	$v=3$	$v=4$	$v=5$	$\langle E_{\rm tot}(J) \rangle$	$\langle E_v \rangle$	$\langle E_r \rangle$	$\langle E_t \rangle$[a]
					Ca + HF($v = 1$)[b]					
0	1.0	0.60	0.27	0.04			5.61	1.10	1.80	2.71
1	1.0	0.61	0.28	0.05			5.73	1.14	1.83	2.76
2	1.0	0.63	0.31	0.08			5.95	1.21	1.87	2.87
3	1.0	0.66	0.35	0.11			6.29	1.31	1.93	3.05
4	1.0	0.71	0.40	0.15	0.01		6.74	1.45	2.00	3.29
5	1.0	0.77	0.46	0.22	0.04		7.31	1.66	2.08	3.57
6	1.0	0.81	0.54	0.29	0.10		7.99	1.90	2.15	3.94
7	1.0	0.84	0.64	0.38	0.17	0.03	8.77	2.20	2.22	4.35
					Ca + DF($v = 2, J$)					
1	1.0	0.86	0.68	0.42	0.21	0.05	9.17	2.35	2.25	4.57
3	1.0	0.86	0.70	0.46	0.24	0.07	9.48	2.46	2.27	4.75
5	1.0	0.88	0.73	0.52	0.30	0.12	10.00	2.64	2.31	5.05

[a] $\langle E_t \rangle$ is calculated from energy conservation.

[b] Based on spectra taken in this study.

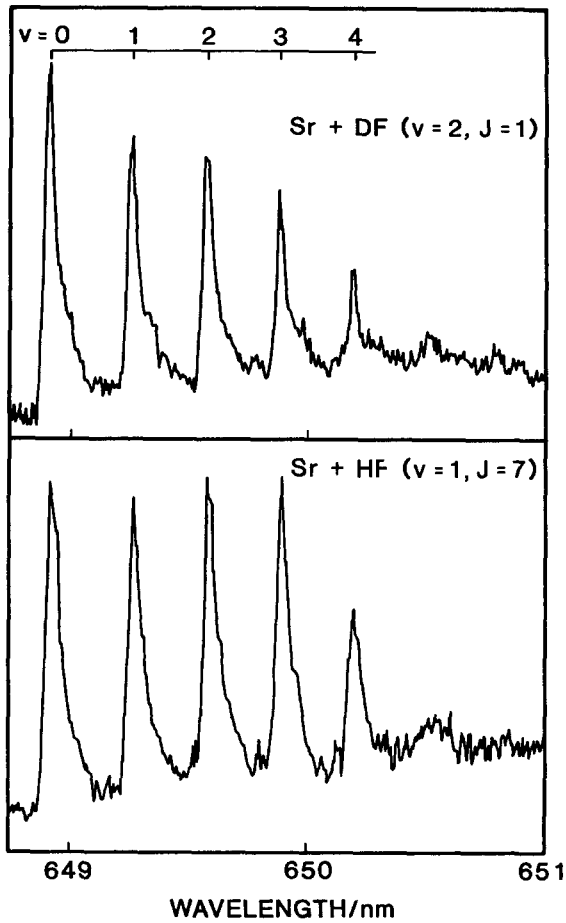

FIG. 6. LIF spectrum of the SrF $X\,^2\Sigma^+$–$A\,^2\Pi_{3/2}$ transition for the reaction: (a) Sr + DF($v=2, J=1$); and (b) Sr + HF($v=1, J=7$).

B. Rotational effects in the Sr+HF reactions

The LIF excitation spectra for the SrF product as a function of the rotational quantum number of HF($v=1$) are shown in Fig. 7. As the HF($v=1, J$) rotational quantum number increases from $J=0$ to $J=7$, two new bandheads appear, corresponding to the formation of SrF in $v=4$ and $v=5$, and the relative populations among the lower levels vary.

Table IV lists the values of the relative vibrational populations P_v found by computer simulation of the SrF product LIF spectra for Sr + HF($v=1, J=0$–7). Also shown in Table IV are the average product vibrational energies $\langle E_v \rangle$, the average product rotational energies $\langle E_r \rangle$ calculated from the values of P_v and $\theta_r(v)$, and the values of $\langle E_{\rm tot}(J) \rangle$.

C. Ca+DF($v=1, J=0$–9) and Sr+DF($v=1, J=0$–9)

From the energy diagrams of Ca + HF(DF) and Sr + HF(DF) reactions shown in Figs. 2 and 3, it can be seen that both the Ca + DF($v=1, J$) and Sr + DF($v=1, J$) reactions are very close to the energetic threshold for reaction. Two effects are observed. First of all, the CaF and SrF products are formed primarily in the $v=0$ state, although there is about 1000 cm^{-1} extra internal energy being put into the system for DF($v=1, J=9$) relative to DF($v=1, J=0$). Figure 8 shows the LIF excitation spectra for the SrF product as a function of the initial rotational levels of DF($v=1$). This is very different from the Ca + HF($v=1, J=0$–7) and the Sr + HF($v=1, J=0$–7) reactions, where two new bandheads appear when the same amount of extra internal energy is put into the system. Second, we find that the reaction rate increases substantially as reagent rotational energy is increased. For example, when DF($v=1$) changes from $J=1$ to $J=8$, the number density of the product increases by approximately a factor of 3.

For these threshold reactions, the spread in the collision energy distribution plays an important role. We suggest the following interpretation of our observations. For low rotational excitation of DF($v=1$), only the tail of the Boltzmann translational energy distribution contributes to the reaction. With higher rotational excitation of DF($v=1$), a larger proportion of the collisions will have sufficient total

TABLE IV. Relative vibration state population of the SrF product P_v with the average total available energy $\langle E_{\rm tot}(J) \rangle$ and its energy partitioning from the Sr + HF($v=1, J$) and Sr + DF($v=2, J$) reactions.

	P_v										
J	$v=0$	$v=1$	$v=2$	$v=3$	$v=4$	$v=5$	$v=6$	$\langle E_{\rm tot}(J) \rangle$	$\langle E_v \rangle$	$\langle E_r \rangle$	$\langle E_t \rangle$[a]
					Sr + HF($v=1$)						
0	1.0	0.69	0.30	0.09				5.02	1.07	1.32	2.63
1	1.0	0.70	0.30	0.11				5.13	1.10	1.35	2.68
2	1.0	0.72	0.38	0.10				5.35	1.15	1.41	2.79
3	1.0	0.74	0.40	0.12				5.69	1.19	1.49	3.01
4	1.0	0.76	0.44	0.13	0.04			6.14	1.31	1.60	3.23
5	1.0	0.75	0.60	0.32	0.10			6.70	1.69	1.65	3.36
6	1.0	0.75	0.64	0.42	0.14	0.02		7.39	1.89	1.73	3.77
7	1.0	0.80	0.75	0.65	0.32	0.13		8.19	2.39	1.58	4.22
					Sr + DF($v=2, J$)						
1	1.0	0.71	0.47	0.29	0.15	0.06		8.57	1.78	1.89	4.90
3	1.0	0.72	0.49	0.31	0.17	0.07	0.01	8.87	1.89	1.88	5.10
5	1.0	0.72	0.51	0.33	0.20	0.09	0.03	9.40	2.03	1.88	5.49

[a] $\langle E_t \rangle$ is calculated from energy conservation.

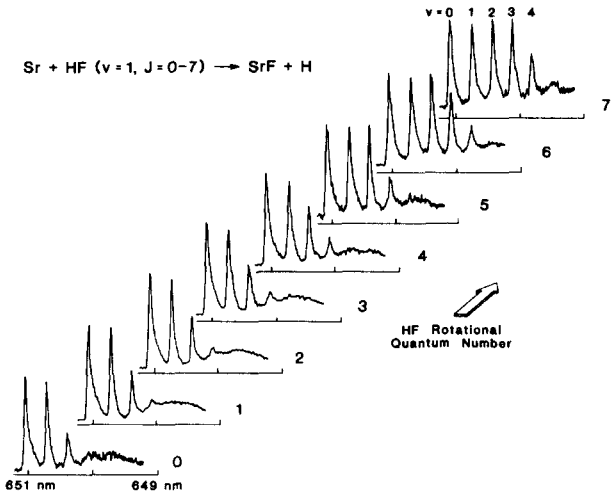

FIG. 7. LIF spectrum of the SrF $X\,^2\Sigma^+$–$A\,^2\Pi_{3/2}$ transition formed in the Sr + HF($v = 1, J$) reactions, as a function of HF rotational quantum number J.

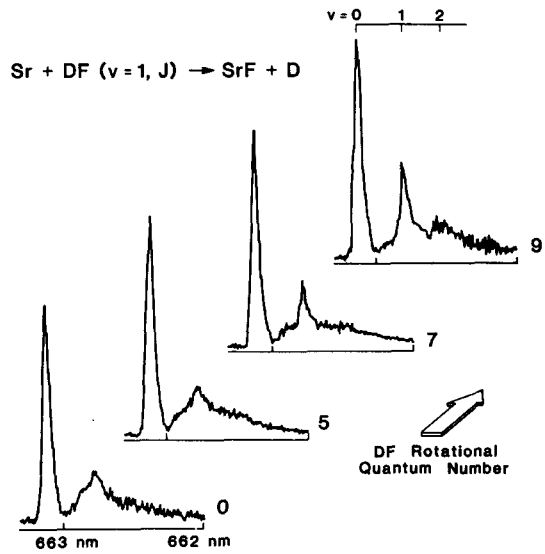

FIG. 8. LIF spectrum of the SrF $X\,^2\Sigma^+$–$A\,^2\Pi_{1/2}$ transition in the Sr + DF($v = 1, J$) reactions, as a function of DF rotational quantum number J.

energy to react causing an increase in the reaction rate. However, the majority of the collisions will still be very close to threshold. This results in production of MF with little internal excitation, i.e., production of primarily MF($v = 0$). To determine whether the low vibrational excitation which is observed is the result of authentically dynamical effects or simply energetic constraints, it would be necessary to perform experiments in which the spread in the collisional energy distribution was significantly reduced.

It should be noted that for the Ca + DF ($v = 1, J$) reactions we are able to resolve the individual rotational lines of the P_2 branch for the CaF (0,0) band because there is little interference from the higher vibrational bands. This is one of the few systems from which information has so far been obtained about the rovibronic state to rovibronic state reaction

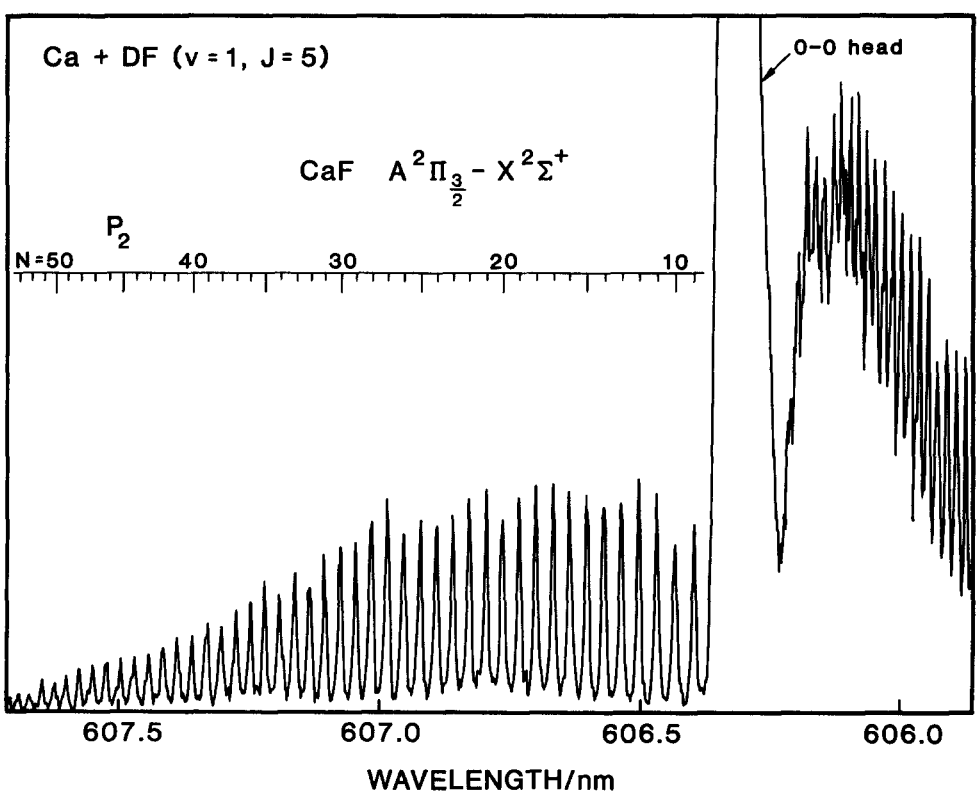

FIG. 9. LIF spectrum of CaF from the Ca + DF($v = 1, J = 4$) reaction showing resolution of individual rotational transitions.

dynamics.[37] Figure 9 illustrates this behavior for the Ca + DF($v=1, J=4$) reaction. However, the spread in the collision energy makes difficult the quantitative deduction of dynamical attributes from the observed product rotational state distribution.

D. Alignment effects

We have measured the relative reaction cross sections and product state distributions for the Sr + HF($v=1, J$) reactions in which we vary the approach geometry by our choice of the directions of the electric vector of the plane polarized OPO output. In this way we can favor collisions in which the Sr atoms are directed to a rotating HF molecule either perpendicular or parallel to the plane of rotation. We observe no significant change in the product state distributions when HF($v=1, J$) is excited via $P(2)$, $R(2)$, $R(3)$, and $R(5)$ transitions, in contradiction to the small effects observed in the preliminary studies of Karny, Estler, and Zare.[7] Furthermore, no change in the absolute cross section is observed (within ~5%) as measured by recording the laser induced fluorescence signal from the (0,0) bandhead while varying the polarization of the OPO output. Similar experiments for Ca + HF($v=1, J$) also show no significant alignment effects.

If the reaction proceeds with a strong preference for either a collinear or a broadside attack geometry, then it would be expected that a pronounced alignment effect would be seen. Indeed, this has been experimentally observed for K + HF($v=1, J=2$) by Hoffmeister, Schleysing, and Loesch.[38] Further support for this picture comes from trajectory studies on sample LEPS surfaces (chosen to be applicable to H + HL systems) by Pattengill, Zare, and Jaffe[39] and for an O + HCl LEPS surface by Schechter, Prisant, and Levine.[40] However, if the minimum energy path involves a bent transition state, then the alignment effect may be substantially reduced for some potential energy surfaces, as seen in the sample LEPS studies of Pattengill *et al.*[39] The Ca + HF potential energy surface has been calculated from first principles and found to prefer a bent transition state for Ca + HF($v=1$). Moreover, trajectory calculations on this surface show a small alignment effect. It might be expected that similar behavior occurs for Sr + HF($v=1$). We suggest that this bent reaction geometry may account, in part, for our observation of no detectable alignment dependence. Any alignment present in these reaction systems would be reduced by our beam–gas experimental conditions, in which the HF velocity vector is randomly distributed in space and the HF molecules are not perfectly aligned.[17,41] [The time-averaged value of the alignment $A_0^{(2)}$ is about -0.46 for $R(2)$ line pumping with linearly polarized radiation].

E. Variation in relative reaction cross section with reagent rotation

Within the accuracy of our measurements (~30%), which include the uncertainties in the amount of HF($v=1$) excited to different J levels as inferred from the optoacoustic measurements, we observe no significant changes in the relative reaction cross section for both Ca + HF($v=1, J$) and Sr + HF($v=1, J$) when we change the initial J of HF($v=1$) from $J=1$ to $J=7$. This result for Ca + HF($v=1, J$) is consistent with the classical trajectory calculations on an *ab initio* surface,[13] which predicts that the relative reaction cross section will increase slightly (a few percent) as the rotational quantum number of the reagent increases. It is also consistent with previous experimental studies in this laboratory.[20,42] For Sr + HF ($v=1, J=1$–3) reactions, Man and Estler[10] measured the relative reaction cross sections and found that they declined by 50% with an experimental precision of 20% in going from $J=1$ to $J=3$. The results of the present study show less change within our precision of 30%.

IV. DISCUSSION

Previous experimental investigations of Ca + HF($v=1, J=0$–7) concluded that the CaF product state distribution was statistical.[11] This result was based on the suitability of a nearly "unbiased" prior distribution for the CaF product spectral simulations. The statistical CaF product distributions are in qualitative agreement with recent quasiclassical trajectory calculations on an *ab initio* surface.[13] These calculations predict that the reaction dynamics are dominated by the formation of long-lived H–Ca–F complexes in which the Ca atom inserts into the HF bond. The present study of Ca + DF($v=2, J$) further supports this reaction mechanism since the CaF distributions are also well represented by statistical distributions. In particular, we find that the nearly isoenergetic reactions Ca + HF($v=1, J=7$) and Ca + DF($v=2, J=1$) give identical product state distributions [see Fig. 10 and the $\langle E_{\rm tot}(J)\rangle$, $\langle E_v\rangle$, and $\langle E_r\rangle$ data in Table III for these two reactions]. This suggests that the reaction retains no "memory" of the initial form of the reagent energy and the excess energy of the reaction is disposed statistically into all possible modes.

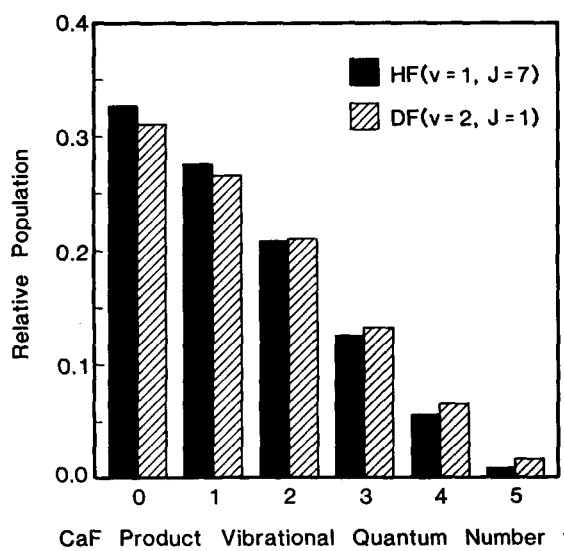

FIG. 10. Relative vibrational state populations of the CaF product from the Ca + HF($v=1, J=7$) reaction (solid) and the Ca + DF($v=2, J=1$) reaction (hatched).

In comparing these two reactions it might be wondered whether there is a significant difference caused by the departure of an H or a D atom. In previous work,[11] a statistical prior distribution has been assumed which was based only on energy conservation [see Eq. (5)] with an angular momentum cutoff. A superior treatment would include conservation of total angular momentum, especially for the present kinematically constrained reaction. Phase space theory considers both energy and angular momentum conservation in predicting the product state distributions.[43–46] We have carried out phase space calculations which take into account the different state densities of the HF/DF reagents and the different reduced masses for the H/D exit channels. The results from the phase space theory calculation are in very good agreement with our experimental results and the results of a prior distribution where an angular momentum cutoff was assumed. Therefore, we conclude that the H/D isotope effect is not dynamically significant.

The Sr + HF(DF) reactions behave very differently from the Ca + HF(DF) reactions. We have found that the product vibrational state distributions for Sr + HF($v = 1, J = 0$–3) are close to the distributions predicted by a statistical prior distribution. These findings are in agreement with the results obtained by Man and Estler[10] who investigated the reaction of strontium with rotational states of HF($v = 1$) only up to $J = 3$. It should be noted that HF($v = 1, J = 3$) represents 0.68 kcal/mol additional rotation energy, which is small compared to 5.7 kcal/mol of the total energy available to the products. We find that the product distribution for the Sr + HF($v = 1$) reaction deviates from a statistical distribution in that it has excess rotational excitation of HF($v = 1$) beyond $J = 3$. For Sr + HF($v = 1, J = 7$) there is 3.2 kcal/mol of rotational energy available to the system, which is a significant fraction of the total energy available to the products of 8.2 kcal/mol. For this reaction, the product distribution differs markedly from the statistical prediction. On the other hand, the nearly isoenergetic reaction of Sr + DF($v = 2, J = 1$) shows a very different behavior. Figure 11 illustrates the SrF product vibrational state distributions for these two systems. The vibrational state distribution for Sr + DF($v = 2, J = 1$) is slightly colder than a statistical prior distribution. In contrast, the SrF vibrational state distribution for Sr + HF($v = 1, J = 7$) is much hotter than a statistical prior distribution. These differences are also apparent in the values of $\langle E_{\text{tot}} \rangle$, $\langle E_v \rangle$, and $\langle E_r \rangle$ given in Table IV.

These differences suggest that the Sr + HF(DF) reaction dynamics are sensitive to the form of the original reagent energy. It appears that the Sr + DF($v = 2, J = 1$) reaction proceeds primarily through a complex which favors statistical formation of the reaction products. Perhaps vibrational excitation of DF enhances Sr atom insertion. The Sr + HF($v = 1$) reaction also appears to be well described as statistical for low rotational excitation, but it deviates dramatically from statistical behavior with increasing HF($v = 1$) rotation. This suggests that direct reaction may be promoted by rotational excitation of the HF($v = 1$) reagent. Thus, it appears in the case of Sr + HF(DF) that a competition exists between direct abstraction vs insertion in the reaction mechanism. This competition may help to explain why reagent vibration is not overwhelmingly more effective than reagent translation in the Sr + HF reaction.[9]

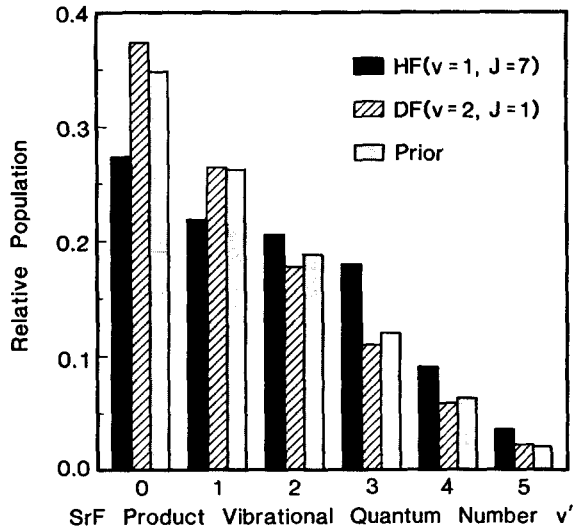

FIG. 11. Relative vibrational state populations of the SrF product from the Sr + HF($v = 1, J = 7$) reaction (solid) and the Sr + DF($v = 2, J = 1$) reaction (hatched) as compared with the relative vibrational state population derived from the statistical prior distribution (shaded).

It is interesting to attempt a reinterpretation of the Ba + HF reaction dynamics in light of what is now known about the Ca + HF(DF) and Sr + HF(DF) reactions. It appears that for low relative initial kinetic energies, the BaF product is nonstatistical[1,3] but becomes more statistical either at higher relative initial kinetic energies[3] or when the HF reagent is vibrationally excited.[4,5] We suggest that this behavior once again reflects a competition between direct reaction at low relative initial kinetic energies and insertion at higher kinetic energies or when the bond being broken is vibrationally excited. Thus, competition between two modes of reaction seems capable of providing a unified picture for the reaction dynamics of alkaline earth atoms with hydrogen fluoride molecules. It is anticipated that these results can be readily generalized to include reactions of the alkaline earth atom with other hydrogen halide molecules. The specific details of the M + HX potential energy surface will determine whether insertion or abstraction is the dominant reaction mechanism for a given set of initial conditions.

ACKNOWLEDGMENTS

We thank J. DeHaven for preliminary work on relative cross sections and alignment effects in the Ca + HF($v = 1, J$) reactions which facilitated the present study. K.G.McK. appreciates the award of a U. K. SERC Postdoctoral Research Fellowship. This work was supported by the U. S. National Science Foundation Grant Nos. NSF 84-07270 and NSF 87-05131.

APPENDIX

Saturation effects

The MF A–X $\Delta v = 0$ bands have relatively large transition probabilities (the radiative lifetime of the CaF A state is

only about 30 ns[16]). Consequently, these transitions may readily be radiatively saturated using probe pulse energies available from the dye laser used in these experiments. In practice, it is found that even with highly attenuated pulse energies as low as 0.6 μJ, there are still clear manifestations of saturation. This pulse energy, which is orders of magnitude less than the maximum available, is the minimum value which retains an adequate signal-to-noise ratio in the excitation spectra of nascent MF products.

Since we are unable to operate in a regime where saturation effects can be avoided, we have made a careful study of the effects of probe pulse energy on the observed excitation spectra in the range 0.6–20 μJ/pulse (bracketing the value of 3 μJ/pulse used in collecting the majority of the data from which product state distributions were derived). For these purposes, the MF produced in the "oven reaction" provides a convenient, stable sample with a known (Boltzmann) population distribution. As the probe pulse energy is increased, it is found that there is a monotonic increase in the width of spectral features, although the spectra remain qualitatively similar. An increasingly less than linear gain in the magnitude of the signal with pulse energy is also apparent.

A further sensitive indication of the extent of saturation is the broadening of the width of individual rotational lines. As explained in Sec. IV, we are able to record CaF spectra which include a resolved, isolated rotational branch (see Fig. 9) for the case of Ca + DF($v = 1, J$). With a pulse energy of 3 μJ, the linewidth in this branch is found to be about 0.6 cm^{-1}, substantially exceeding the time-averaged dye laser bandwidth of about 0.1 cm^{-1}. With higher pulse energies, the lines of this branch become broader and poorly resolved.

Clearly, simulations of the excitation spectra which do not include the effects of saturation will fail to reproduce certain aspects of the experimental observations. Population information deduced from such oversimplified modeling will correspondingly be somewhat suspect. In the unsaturated limit, the linewidth of individual transitions is simply equal to the laser bandwidth. (The Doppler width, about 0.02 cm^{-1}, is sufficiently small to be effectively negligible.) Even in cases where spectral congestion prevents the individual linewidth from being apparent, discrepancies between the experimental results and simulations in which an appropriate fixed linewidth is assumed are still obvious. The disagreement is particularly marked in the shape of the short wavelength edges of the rotational bandheads, which are predicted to be too "sharp."

In the general case where both the laser bandwidth and saturation broadening contribute significantly to the observed linewidth, the line shape will depend in a rather complicated fashion on the details of the mode structure of individual pulses. However, as noted above, with a pulse energy of 3 μJ, the power broadened linewidth (about 0.6 cm^{-1}) of isolated P_2 branch lines is some six times greater than the laser bandwidth.

Therefore, we have constructed simulated spectra in which the simplyfing assumption is made that the linewidth is determined entirely by saturation broadening. We find improved and satisfactory agreement with experiment over the pulse energy range of interest. The line shape in this case is Lorentzian, with a width determined by the absolute transition probability (Einstein B coefficient) and the radiative energy density. The Einstein B coefficients for individual lines are simply calculated from the radiative lifetime of the MF A state, the Franck–Condon factors, and the rotational line strengths.[35] Note that the resulting linewidth is dependent on the strength of the line. Although it is possible, in principle, to calculate the absolute energy density from the measured pulse energy, in practice the spatial distribution of our probe beam is not sufficiently well defined to make this an accurate procedure. Instead, we treat the energy density as being characterized by a single adjustable parameter, the value being fixed by optimization of the agreement between synthetic and observed spectra at a pulse energy of 3 μJ. It is then found that the spectra at other pulse energies are reproduced very satisfactorily by simulations using the correct relative values of the energy density.

[1] H. W. Cruse, P. J. Dagdigian, and R. N. Zare, Faraday Discuss. Chem. Soc. **55**, 277 (1973).
[2] J. G. Pruett and R. N. Zare, J. Chem. Phys. **64**, 1774 (1976).
[3] A. Gupta, D. S. Perry, and R. N. Zare, J. Chem. Phys. **72**, 6237 (1980).
[4] A. Torres-Filho and J. G. Pruett, J. Chem. Phys. **72**, 6736 (1980).
[5] A. Torres-Filho and J. G. Pruett, J. Chem. Phys. **77**, 740(1982).
[6] Z. Karny and R. N. Zare, J. Chem. Phys. **68**, 3360 (1978).
[7] Z. Karny, R. C. Estler, and R. N. Zare, J. Chem. Phys. **69**, 5199 (1979).
[8] D. S. Perry, A. Gupta, and R. N. Zare, Electro-Optic Laser '80, Proceedings (Industrial & Scientific Management, Chicago, 1981).
[9] A. Gupta, D. S. Perry, and R. N. Zare, J. Chem. Phys. **72**, 6250 (1980).
[10] C. K. Man and R. C. Estler, J. Chem. Phys. **75**, 2779 (1981).
[11] R. I. Altkorn, F. E. Bartoszek, J. DeHaven, G. Hancock, D. S. Perry, and R. N. Zare, Chem. Phys. Lett. **98**, 212 (1983).
[12] C. Noda, J. S. McKillop, M. A. Johnson, J. R. Waldeck, and R. N. Zare, J. Chem. Phys. **85**, 856 (1986).
[13] R. L. Jaffe, M. D. Pattengill, F. G. Mascarello, and R. N. Zare, J. Chem. Phys. **86**, 6150 (1987).
[14] K. G. Anlauf, D. H. Maylotte, J. C. Polanyi, and R. B. Bernstein, J. Chem. Phys. **51**, 5716 (1969); J. C. Polanyi and D. C. Tardy, *ibid.* **51**, 5717 (1969); D. S. Perry, J. C. Polanyi, and C. W. Wilson, Jr., Chem. Phys. Lett. **24**, 484 (1974); D. S. Perry and J. C. Polanyi, Chem. Phys. **12**, 419 (1976).
[15] J. J. Hinchen, J. Opt. Soc. Am. **64**, 1162 (1974).
[16] P. J. Dagdigian, H. W. Cruse, and R. N. Zare, J. Chem. Phys. **60**, 2330 (1974).
[17] R. N. Zare, Ber. Bunsenges. Phys. Chem. **86**, 422 (1982).
[18] C. Kittel and H. Kroemer, *Thermal Physics*, 2nd ed. (W. S. Freeman, San Francisco, 1980).
[19] R. N. Porter and L. M. Raff, in *Dynamics of Molecular Collisions. Part B*, edited by W. H. Miller (Plenum, New York, 1976).
[20] R. I. Altkorn, Ph.D thesis, Stanford University, 1984.
[21] R. W. Field, D. O. Harris, and T. Tanaka, J. Mol. Spectrosc. **57**, 107 (1975).
[22] J. Nagakawa, P. J. Domaille, T. C. Steimle, and D. O. Harris, J. Mol. Spectrosc. **70**, 374 (1978).
[23] M. Dulick, P. F. Bernath, and R. W. Field, Can. J. Phys. **58**, 703 (1980).
[24] W. J. Childs and L. S. Goodman, Phys. Rev. A **21**, 1216(1980).
[25] W. J. Childs, G. L. Goodman, and L. S. Goodman, J. Mol. Spectrosc. **86**, 365 (1981).
[26] G. Herzberg, *Molecular Spectra and Molecular Structure*, Vol 1. *Spectra of Diatomic Molecules*, 2nd ed. (Van Nostrand, New York, 1950).
[27] R. D. Levine and R. B. Bernstein, *Molecular Reaction Dynamics and Chemical Reactivity* (Oxford University, Oxford, 1987).
[28] M. M. Novikov and L. V. Gurvich, Opt. Spectrosc. **20**, 365 (1967).
[29] T. C. Steimle, P. J. Domaille, and D. O. Harris, J. Mol. Spectrosc. **68**, 134 (1977).
[30] P. J. Domaille, T. C. Steimle, and D. O. Harris, J. Mol. Spectrosc. **68**, 146 (1977).

[31]T. C. Steimle, P. J. Domaille, and D. O. Harris, J. Mol. Spectrosc. **73**, 441 (1978).
[32]R. S. Ram, S. B. Rai, and K. N. Upadhya, Pramana. **15**, 413 (1980).
[33]W. E. Ernst and J. O. Schroder, Chem. Phys. **78**, 363 (1983).
[34]The Franck–Condon factors, $q_{v',v''}$ used for both CaF and SrF are: $q_{0,0} = 0.978$; $q_{1,1} = 0.936$; $q_{2,2} = 0.896$; $q_{3,3} = 0.858$; $q_{4,4} = 0.822$; $q_{5,5} = 0.788$; $q_{6,6} = 0.756$. The values for $q_{0,0}$–$q_{2,2}$ have been obtained from Ref. 6 and the others by extrapolation.
[35]Line strengths calculated by using the formula developed by L. T. Earls, in Phys. Rev. **48**, 423 (1935).
[36]R. D. Levine and J. L. Kinsey, in *Atom–Molecule Collision Theory. A Guide for the Experimentalist*, edited by R. B. Bernstein (Plenum, New York, 1979).
[37]D. J. Rakestraw, K. G. McKendrick, and R. N. Zare, J. Chem. Phys. **87**, 7341 (1987).
[38]M. Hoffmeister, R. Schleysing, and H. Loesch, J. Phys. Chem. **91**, 5441 (1987).
[39]M. D. Pattengill, R. N. Zare, and R. L. Jaffe, J. Phys. Chem. **91**, 5489 (1987).
[40]I. Schechter, M. G. Prisant, and R. D. Levine, J. Phys. Chem. **91**, 5472 (1987).
[41]R. Altkorn, R. N. Zare, and C. H. Greene, Mol. Phys. **55**, 1 (1985).
[42]J. DeHaven (unpublished experimental results).
[43]J. C. Light, J. Chem. Phys. **42**, 3221 (1964).
[44]P. Pechukas and J. C. Light, J. Chem. Phys. **42**, 3281 (1964).
[45]P. Pechukas, J. C. Light, and C. Rankin, J. Chem. Phys. **44**, 794 (1966).
[46]P. J. Dagdigian, H. W. Cruse, A. Schultz, and R. N. Zare, J. Chem. Phys. **61**, 4450 (1974).